A 0.044-mm2 0.5-to-7-GHz resistor-plus-source-follower-feedback noise-cancelling LNA achieving a flat NF of 3.3±0.45 dB

Yu, Haohong; Chen, Yong; Boon, Chirn Chye; Li, Chenyang; Mak, Pui-In; Martins, Rui P.

2019

Yu, H., Chen, Y., Boon, C. C., Li, C., Mak, P.-I., & Martins, R. P. (2019). A 0.044-mm2 0.5-to-7-GHz resistor-plus-source-follower-feedback noise-cancelling LNA achieving a flat NF of 3.3±0.45 dB. IEEE Transactions on Circuits and Systems II: Express Briefs, 66(1), 71-75. doi:10.1109/TCSII.2018.2833553

https://hdl.handle.net/10356/102668

https://doi.org/10.1109/TCSII.2018.2833553

A 0.044-mm^2 0.5-to-7-GHz Resistor-Plus-Source-Follower-Feedback Noise-Cancelling LNA Achieving a Flat NF of 3.3±0.45 dB

Haohong Yu, Yong Chen, *Member, IEEE*, Chirn Chye Boon, *Senior Member, IEEE*, Chenyang Li, Pui-In Mak, *Senior Member, IEEE*, and Rui P. Martins, *Fellow, IEEE*

***Abstract*—A wideband noise-cancelling low-noise amplifier (LNA) combining resistor feedback and source-follower feedback (SFF) is proposed. The SFF facilitates upsizing of the feedback resistor to improve the gain and noise figure (NF), without compromising the input-impedance matching. Another benefit is that the noise contributions of both the feedback resistor and noise-cancelling transistors are significantly reduced. Fabricated in 65-nm CMOS, the LNA exhibits a voltage gain of 16.8 dB, and a flat NF of 3.3 ± 0.45 dB over a −3-dB bandwidth of 0.5 to 7 GHz. The power consumption is 11.3 mW at 1.2 V, and the die area is 0.044 mm^2.**

***Index Terms*—Noise cancelling, low-noise amplifier (LNA), source follower feedback (SFF), resistor feedback, CMOS, noise figure (NF), wideband input impedance matching.**

I. Introduction

WIDEBAND receivers are promising to support high-rate data communication [1], [2], or multiple wireless standards distributed over the sub-6-GHz RF spectrum [3]–[6]. Especially in the ultra-scale CMOS technologies, the transistor features an adequate f_T to serve as a wideband RF low-noise amplifier (LNA) with high gain, low noise figure (NF) and good linearity [2]–[14]. A single-transistor LNA with resistive feedback can easily achieve a wideband input return loss (S_{11}) <-10 dB. However, both the gain and NF are sub-optimal due to the S_{11} tradeoff with the transistor's transconductance (∼20 mS) [15]. Thus, recent wideband LNAs also introduce noise cancellation [2]–[6], [12], [13] to alleviate the tradeoff between NF and S_{11}. In this brief, a source-follower feedback (SFF) is introduced to alleviate the performance tradeoffs of the resistive-feedback noise-cancelling LNA. The source follower senses the output voltage and returns a negative current back to the input. Effectively, this adds a shunt load at the gate of the input-matching transistor and thereby allows a large feedback resistor to improve the overall gain and NF. With an active area of 0.045 mm^2 and power consumption of 11.3 mW, the LNA prototyped in 65-nm CMOS achieves a competitive figure-of- merit (FOM) [4] of 3.57.

Section II describes the proposed LNA in details. Section III discusses its performances with and without the SFF. Section IV presents the measurement results, and the conclusions are drawn in Section V.

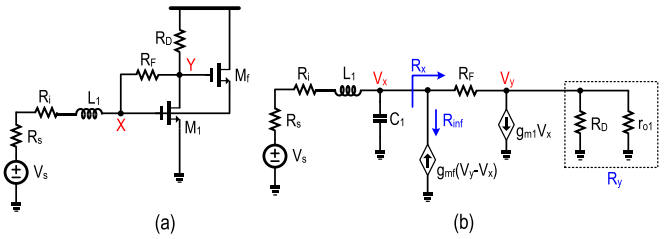

Fig. 1. (a) Schematic and (b) small-signal equivalent circuit of the proposed resistive-feedback LNA with additional SFF.

II. Proposed Resistor-Plus-SFF LNA

A. Wideband Input-Impedance Matching

To alleviate the tradeoff between S_{11}, gain and NF, a local SFF (M_f) is added to a resistive-feedback LNA between X and Y as shown in Fig. 1(a). In addition, a series inductor is connected to the gate of M_1 to broaden the input-matching bandwidth (BW) [2]. Note that the DC biasing circuit is omitted for clarity. The S_{11} derived from Fig. 1(b) is given by

$$S_{11} = \left| \frac{L_1 C_1 R_s s^2 + (L_1 + C_1 R_x R_i - C_1 R_x R_s)s + R_x + R_i - R_s}{L_1 C_1 R_s s^2 + (L_1 + C_1 R_x R_i - C_1 R_x R_s)s + R_x + R_i + R_s} \right| \quad (1)$$

Manuscript received November 13, 2017; revised February 2, 2018; accepted May 3, 2018. Date of publication May 7, 2018; date of current version December 20, 2018. This work was supported by the Singapore Ministry of Education Academic Research Fund Tier 1 under Grant MOE RG86/16. This brief was recommended by Associate Editor V. Saxena. *(Corresponding author: Yong Chen.)*

H. Yu, C. C. Boon, and C. Li are with the School of Electrical and Electronic Engineering, Nanyang Technological University, Singapore 639798 (e-mail: yuha0012@e.ntu.edu.sg).

Y. Chen is with the State-Key Laboratory of Analog and Mixed-Signal VLSI, University of Macau, Macau 999078, China (e-mail: ychen@umac.mo).

P.-I. Mak is with the State-Key Laboratory of Analog and Mixed-Signal VLSI, University of Macau, Macau 999078, China, and also with the Faculty of Science and Technology, Department of ECE, University of Macau, Macau 999078, China (e-mail: pimak@umac.mo).

R. P. Martins is with the State-Key Laboratory of Analog and Mixed-Signal VLSI, University of Macau, Macau 999078, China, with the Faculty of Science and Technology, Department of ECE, University of Macau, Macau 999078, China, and also on leave from Instituto Superior Técnico, Universidade de Lisboa, 1049-001 Lisbon, Portugal (e-mail: rmartins@umac.mo).

Color versions of one or more of the figures in this paper are available online at http://ieeexplore.ieee.org.

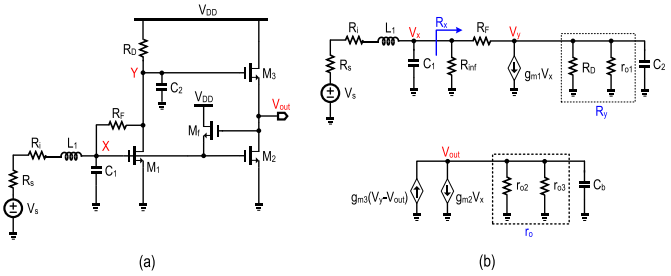

Fig. 2. (a) Schematic and (b) small-signal equivalent circuit of the proposed LNA combining local source-follower-based feedback with noise-cancelling technique.

where L_1 is the matching inductor, R_i is its parasitic resistance, C_1 is the parasitic capacitance at X and R_x is the resistance looking into X in Fig. 1(b). Due to the addition of SFF, R_x in Fig. 1(b) is expressed as

$$R_x = \frac{(R_y + R_F)R_{inf}}{(g_{m1}R_y + 1)R_{inf} + R_y + R_F} \tag{2a}$$

where

$$\mathrm{R_{inf}} = \frac{1}{g_{mf}(1 - V_y/V_x)} \tag{2b}$$

and $R_y = R_D||r_{01}$ as shown in Fig. 1(b). R_x is smaller than the typical resistive-feedback LNA due to the term $R_y + R_F$ in the denominator. Since V_y/V_x is negative, it leads to a negative $g_{mf}(V_y - V_x)$. Thus, a small-signal current in M_f flows from X to ground, making M_f an effective resistor (R_{inf}), lowering the input impedance of the LNA. Thus, a larger R_F can be employed without compromising input matching. A larger R_F benefits both the gain and NF, as detailed later.

B. Frequency Response of S_{21}

Noise-cancelling technique is common in a wide-band LNA to improve the NF and gain. Fig. 2(a) and (b) show, respectively, the schematic (without DC bias network) and small-signal equivalent circuit of the proposed LNA with a source follower (M_f) and noise-cancelling paths (M_2 and M_3). C_1 and C_2 represent the total parasitic capacitances at X and Y, respectively. The total voltage gain consists of two parts: $A_1 = V_x/V_s$ and $A_v = V_{out}/V_x$. A_1 is the voltage gain from the source to X, which can be written as

$$A_1 = \frac{R_x}{L_1C_1R_xs^2 + [L_1 + C_1R_x(R_s + R_i)]s + R_s + R_x + R_i} \tag{3}$$

where R_x is given by (2a). Yet, the resistance looking into the source of M_f is slightly changed, $R_{inf} = 1/g_{mf}(1 + |A_v|)$. From (3), the reactive components that mainly determine the poles of A_1 are C_1 and L_1. Typically $C_2 << C_1$ since M_3 is designed smaller than M_1 and M_2 for noise-cancelling purpose. The effect of C_2 on A_1 is neglected for simplicity. The second part (A_v) of the overall LNA gain is the voltage gain from X to the output node and is given by

$$\mathrm{A_v} = -\frac{(-g_{m3}A_2 + g_{m2})(r_0||C_b)}{1 + g_{m3}(r_0||C_b)} \tag{4a}$$

where

$$A_2 = \frac{V_y}{V_x} = -\frac{R_FR_yg_{m1} - R_y}{C_2R_FR_ys + R_y + R_F} \tag{4b}$$

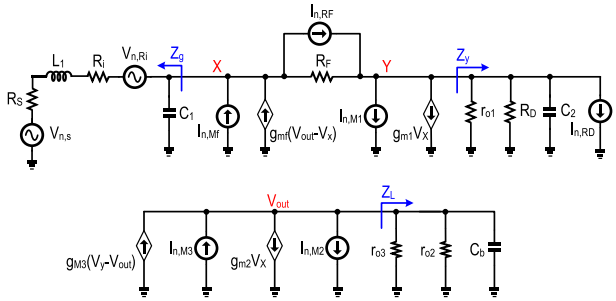

Fig. 3. Equivalent circuit of Fig. 2(a) for noise calculation.

and $r_0 = r_{02}||r_{03}$. A_2 is the voltage gain from X to Y. g_{m2}, g_{m3}, r_{02} and r_{03} are the transconductance of M_2 and M_3 and drain-source resistance of M_2 and M_3, respectively. C_b is the gate capacitance of the testing buffer. If we assume $1 + g_{m3}r_0 \approx g_{m3}\, r_0$, which is usually the case, (4a) can be simplified as $A_v = A_2 - g_{m2}/g_{m3}$. Note that A_2 is negative and it is clear that the noise-cancelling technique also improves the gain. S_{21} is twice the gain in a 50-Ω system with impedance matching and it is given by

$$S_{21} = 2A_{core} = 2A_1A_v \tag{5}$$

where A_{core} is the total voltage gain from the source to the output in Fig. 2, and $A_{core} = A_vA_1$. Equations (2), (3) and (4) show that adding M_f only affects A_1 and has no influence on A_v. Under an matched input-impedance, i.e., $A_1 = 0.5$ at DC, S_{21} has the same expression for both situations with and without M_f. However, with the presence of M_f, R_F can be upsized when comparing it with the non-feedback case. Thus, from (4), a larger R_F benefits the gain.

C. Frequency Response of NF

The main noise sources of the LNA are the channel resistance thermal noises from M_1, M_2, M_3 and M_f, as well as the thermal noises from R_D and R_F. The noise contributed by the input inductor parasitic resistance R_i is also taken into account. Fig. 3 shows the small-signal equivalent circuit of Fig. 2(a) for noise calculation. The noise factor of M_1 is given by

$$F_{M1} = \frac{g_{m1}}{R_s|A_{core}|^2}\frac{\gamma}{\alpha}\left|\frac{R_FA_{v,n1}}{\left(1 + \frac{R_F}{Z_y}\right)A_{1,n1} + R_Fg_{m1} - 1}\right| \tag{6a}$$

where

$$A_{1,n1} = \frac{V_{y,n1}}{V_{x,n1}} = 1 + \frac{R_F}{Z_g} + g_{mf}R_F\frac{\frac{g_{m2}}{g_{m3}} + \frac{1}{g_{m3}Z_L} - \frac{R_F}{Z_g}}{1 + \frac{1}{g_{m3}Z_L} + R_Fg_{mf}} \tag{6b}$$

$$A_{v,n1} = \frac{V_{out,n1}}{V_{x,n1}} = \frac{g_{mf}R_F + \frac{R_F}{Z_g} + 1 - \frac{g_{m2}}{g_{m3}}}{g_{mf}R_F + \frac{1}{Z_Lg_{m3}} + 1} \tag{6c}$$

As shown in Fig. 3, $Z_y = R_y/(C_2R_ys+1)$, $Z_L = r_o/(C_br_0s+1)$, and $Z_g = (L_1s + R_s + R_i)/(L_1C_1s^2 + C_1(R_s + R_i)s + 1)$. Z_y is the impedance of R_y parallel with C_2. Z_g is the impedance looking into the matching network from X. Z_L is the total impedance at V_{out}. $A_{1,n1}$ is the ratio of noise voltage caused by M_1 at Y to that at X. $A_{v,n1}$ is the ratio of noise voltage caused by M_1 at V_{out} to that at X. γ is the coefficient of channel noise and $\alpha = g_{m1}/g_{d0}$, where g_{d0} is zero-bias drain conductance. Equation (6c) shows that perfect noise cancelling

is achieved when $g_{mf}R_F + R_F/Z_g + 1 = g_{m2}/g_{m3}$, leading to $F_{M1} = 0$. However, since Z_g is complex and g_{m2}/g_{m3} is real, a perfect noise cancellation cannot be accomplished. A good approximation is $\Re(g_{mf}R_F + R_F/Z_g + 1) = g_{m2}/g_{m3}$. As shown in Fig. 3, both $I_{n,RD}$ and $I_{n,M1}$ flow from node Y to ground, therefore the transfer functions from $I_{n,M1}$ and $I_{n,RD}$ to the output are the same. Both $I_{n,M2}$ and $I_{n,M3}$ flows from V_{out} to ground, so a similar case is true for $I_{n,M2}$ and $I_{n,M3}$. Then, the noise factor of R_D, M_2 and M_3 will become:

$$F_{RD} = \frac{1}{R_D g_{m1}} F_{M1} \tag{7}$$

$$F_{M2} = \frac{g_{m2}}{R_s |A_{core}|^2} \frac{\gamma}{\alpha} \times \left| Z_L - \frac{g_{m3} Z_L \left(A_{v,n2} - A_{1,n2}\right) + g_{m2} Z_L}{g_{m3} Z_L \left(A_{v,n2} - A_{1,n2}\right) + g_{m2} Z_L + A_{v,n2}} \right|^2 \tag{8a}$$

where

$$A_{1,n2} = \frac{V_{y,n2}}{V_{x,n2}} = -\frac{R_y (R_F g_{m1} - 1)}{C_2 R_F R_y s + R_F + R_y} \tag{8b}$$

$$A_{v,n2} = \frac{V_{out,n2}}{V_{x,n2}} = 1 + \frac{1}{g_{mf}} \frac{L_1 C_1 s^2 + C_1 R_s s + 1}{L_1 s + R_s} + \frac{1}{g_{mf}} \frac{C_2 R_y s + R_y g_{m1} + 1}{C_2 R_F R_y s + R_F + R_y} \tag{8c}$$

$$F_{M3} = \frac{g_{m3}}{g_{m2}} F_{M2} \tag{9}$$

$V_{x,n2}$, $V_{y,n2}$, and $V_{out,n2}$ are the noise voltages caused by M_2 at X, Y and V_{out} , respectively. To analyze the effect of feedback on F_{M2}, the noise factor contributed by M_2 under non-feedback condition can be calculated as

$$F_{M2,wofb} = \frac{g_{m2}}{R_s \left|A_{core,wofb}\right|^2} \frac{\gamma}{\alpha} |Z_L|^2 \tag{10}$$

Since $A_{1,n2}$ is negative and $|A_{core}| > |A_{core,wofb}|$, F_{M2} and F_{M3} are reduced with the aid of M_f.

The noise factor contributed by feedback resistor R_F is

$$F_{RF} = \frac{1}{R_F R_s |A_{core}|^2} \cdot \left| \frac{A_{v,RF}}{\frac{1}{Z_g} + g_{mf}\left(1 - A_{v,RF}\right) + \frac{1 - A_{1,RF}}{R_F}} \right|^2 \tag{11a}$$

where

$$A_{1,RF} = \frac{V_{y,RF}}{V_{x,RF}} = -\frac{Z_y}{Z_g} - g_{m1} Z_y + g_{mf} \frac{g_{m3} Z_L \left(\frac{Z_y}{Z_g} + g_{m1} Z_y + 1\right) + g_{m2} Z_L + 1}{g_{m3} Z_L \left(g_{mf} - \frac{1}{Z_y}\right) - \frac{1}{Z_y}} \tag{11b}$$

$$A_{v,RF} = \frac{V_{out,RF}}{V_{x,RF}} = -\frac{Z_L \left(g_{m3} \frac{Z_y}{Z_g} + g_{m1} g_{m3} Z_y + g_{m2}\right)}{1 + g_{m3} Z_L} + \frac{g_{mf} g_{m3} Z_L}{1 + g_{m3} Z_L} \frac{g_{m3} Z_L \left(\frac{Z_y}{Z_g} + g_{m1} Z_y + 1\right) + g_{m2} Z_L + 1}{g_{m3} Z_L \left(g_{mf} - \frac{1}{Z_y}\right) - \frac{1}{Z_y}} \tag{11c}$$

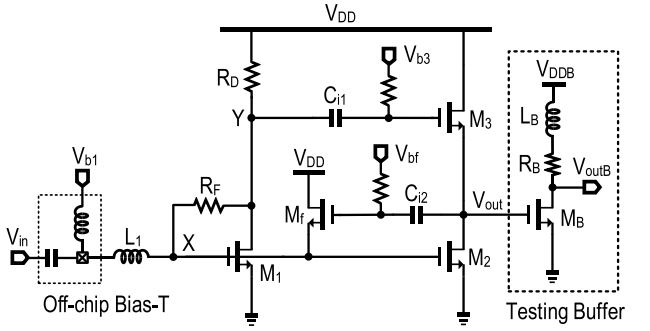

M_1	140µm/65nm	M_3	20µm/65nm	M_B	120µm/65nm	R_D	135Ω	L_1	0.54nH
M_2	159µm/65nm	M_f	3µm/65nm	R_F	640Ω	R_B	40Ω	L_B	1.50nH
I_{M1}	4.9 mA	I_{M2}	4.7 mA	I_{Mf}	117 µA				

Fig. 4. Complete schematic of the proposed wideband LNA.

$V_{x,RF}$, $V_{y,RF}$ and $V_{out,RF}$ are the noise voltage caused by R_F at X, Y and V_{out}, respectively. The term $g_{mf}(1 - A_{v,RF})$, which is introduced by M_f, in the denominator of (11a) reduces F_{RF}. Moreover, the term $\frac{1}{R_F}|\frac{A_{v,RF}}{\frac{1}{Z_g} + g_{mf}(1 - A_{v,RF}) + \frac{1 - A_{1,RF}}{R_F}}|^2$ decreases with increasing R_F. Since adding M_f allows larger R_F and $|A_{core}|$, F_{RF} is also improved. One drawback of adding active feedback loop in LNA is the extra noise brought by M_f as given by:

$$F_{Mf} = \frac{g_{mf}}{R_s |A_{core}|^2} \frac{\gamma}{\alpha} \times \left| \frac{Z_g A_{v,nmf}}{\left(g_{mf} Z_g A_{v,nmf} - g_{mf} Z_g - 1\right) + \frac{Z_g \left(A_{1,nmf} - 1\right)}{R_F}} \right|^2 \tag{12a}$$

where

$$A_{1,nmf} = \frac{V_{y,Mf}}{V_{x,Mf}} = \frac{Z_y (1 - R_F g_{m1})}{R_F + Z_y} \tag{12b}$$

$$A_{v,nmf} = \frac{V_{out,Mf}}{V_{x,Mf}} = \frac{Z_L}{1 + g_{m3} Z_L} \times \frac{g_{m3} Z_y - g_{m2} Z_y - g_{m2} R_F - g_{m1} g_{m3} R_F Z_y}{R_F + Z_y} \tag{12c}$$

$V_{x,Mf}$, $V_{y,Mf}$ and $V_{out,Mf}$ are the noise voltage caused by M_f at X, Y and V_{out}, respectively. F_{Mf} increases along with R_F according to (12a). This potentially limits the improvement of NF. Yet, F_{Mf} is still buffered by an enhanced $|A_{core}|$. Moreover, it only contributes a small portion in total noise factor, as shown in the next section. The overall noise factor will be:

$$F = 1 + \frac{R_i}{R_s} + F_{M1} + F_{RD} + F_{M2} + F_{M3} + F_{RF} + F_{Mf} \tag{13}$$

By noise cancellation, the noise from M_1 and R_D is reduced. Also, all F_{RF}, F_{M2} and F_{M3} are decreased due to local SFF.

III. Proposed Complete LNA

Fig. 4 shows the complete schematic of the LNA, where we used capacitors $C_{i1}$and C_{i2} for DC-decoupling and voltages V_{b3} and V_{bf} to bias the transistors M_3 and M_f, respectively. The gate bias (V_{b1}) of M_1 and M_2, provided by an off-chip bias-T, also biases the source of M_f. The DC current of M_f flows from V_{DD} to V_{b1}. A common-source output buffer is added to provide output matching for measurements. An inductor

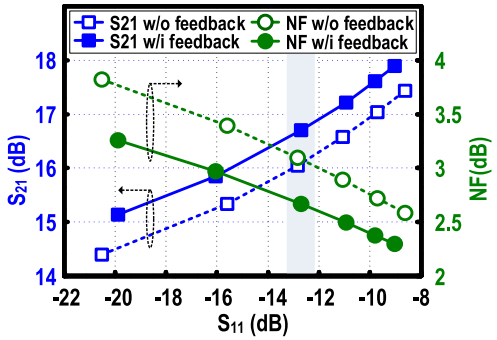

Fig. 5. Simulated NF and S_{21} versus S_{11} of the LNAs with and without the local SFF at 3 GHz.

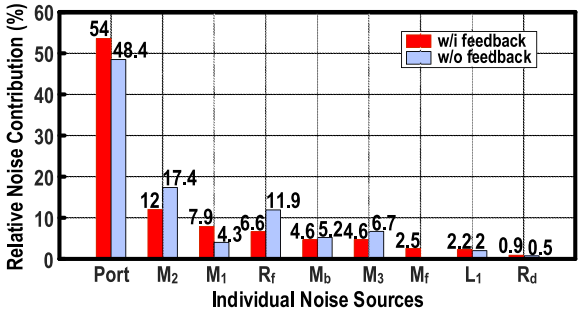

Fig. 6. Simulated relative noise contributions by individual components in the LNAs with and without local SFF.

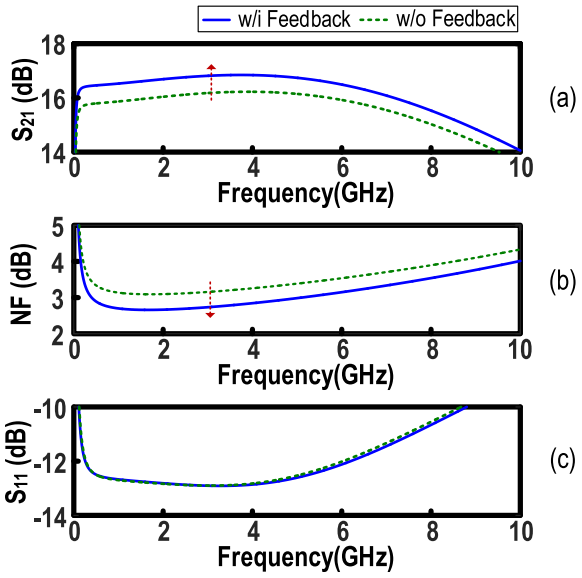

Fig. 7. Simulated (a) S_{21} and (b) NF versus frequency of the LNAs with and without local SFF, under the same (c) input matching condition.

L_B is series connected to the drain of the buffer transistor to counter the effect of the load capacitance on LNA core's bandwidth. Simulations are performed to verify the performance enhancement introduced by M_f. Fig. 5 illustrates the circuit performance of the LNA with and without feedback at various S_{11}. R_F is swept to obtain the various matching conditions. The maximum improvement of gain and NF are 0.9 and 0.57 dB, respectively. Across a wide range of matching conditions, from -20 to -8 dB, the proposed LNA with feedback always has

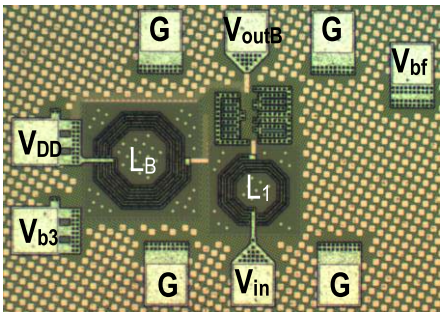

Fig. 8. Die photo of the proposed LNA.

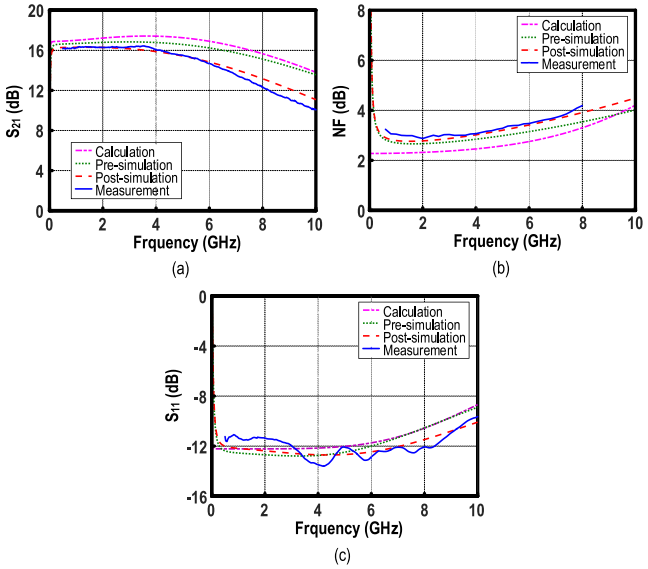

Fig. 9. Calculated, simulated and measured (a) S_{21}, (b) NF and (c) S_{11} versus frequency of the proposed LNA. Pre-simulation is pre-layout simulation and post-simulation is post-layout simulation considering the parasitic effects.

a better S_{21} and NF than the LNA without feedback. The feedback loop is unconditionally stable in the simulations.

Fig. 6 presents the relative noise contributions by individual components in the LNA with and without feedback. With M_f, the noise contribution percentages of M_2, R_F, and M_3 drop from 17.4%, 11.9% and 6.7% to 12.0%, 6.6% and 4.6%, respectively. The reduction of noise contribution is consistent with the analysis in Section II. The noise from M_f is 2.5%, which is relatively small when compared with the total noise reduction in other components. Although noise from M_1 is higher than the non-feedback situation, adding M_f into the LNA improves the overall NF, which is reflected by the port noise contribution. Fig. 7 shows, at the same input matching of -12.5 dB, that the proposed LNA with feedback M_f has better S_{21} and NF performance than the LNA without feedback. When both LNAs show a S_{11} of -12.5 dB, R_F in the non-feedback LNA is 300 Ω, while R_F in our proposed LNA is 640 Ω. As discussed in Section II, a higher R_F improves both the gain and NF. S_{21} and NF are improved by 0.7 and 0.45 dB, respectively.

IV. Measurement Results

The LNA fabricated in 65-nm CMOS occupies a die area of 0.25 x 0.18 mm^2(Fig. 8). It draws 11.3 mW at a single 1.2-V

TABLE I
PERFORMANCE SUMMARY AND BENCHMARK WITH THE STATE-OF-THE-ART

	CMOS	Frequency (GHz)	BW (GHz)	Gain (dB) @ GHz	NF (dB)	NF_{min} (dB)	IIP3 (dBm) @ GHz	Supply Voltage (V)	Power (mW)	Area (mm^2)	FOM*
This Work	65nm	0.5 – 7	6.5	16.8 @ 4	2.87 – 3.77	2.87	-4.5 @ 4	1.2	11.3	0.044	3.57
[4] TCAS-I'12	65nm	0.1 – 5.3	5.2	10.7 @ 1	2.9 – 5.4	2.9	-6 @ 1	1	7	0.03	-3.43
[5] MWCL'15	65nm	0.1 – 2.5	2.4	18 @ 0.5	1.7 – 2.7	1.7	-3 @ 2.2	1.2	13	0.008	3.71
[6] ESSCIR'10	65nm	0.1 – 4.0	3.9	18 @ 0.5	2 – 4.4	2	-5.5 @ 1	1.2	12	0.001	1.9
[7] TCAS-II'10	90nm	3.0 – 8.5	5.5	16 @ 3	3.1 – 4.4	3.1	-5.4 @ 5	1.2	16	0.022	-4.43
[8] JSSC'10	130nm	2.1 – 3.4	1.3	16.4 @ 0.7	2.1 – 3.4	2.1	0 @ 0.9	1.8	14.4	0.036	-1
[11] TMTT'16	130nm	0.1 – 2.2	2.1	12.3 @ 0.2	4.9 – 6	4.9	-10.5 @ 1	1	0.4	0.005	-0.70
[12] TMTT'10	180nm	1.7 – 5.9	4.2	13.5 @ 3.5	3.6 – 4.7	3.6	-12 @ 6	1.8	10.34	0.565	-20.5
[13]TCAS-II'13	180nm	0.5 – 1.3	0.8	10 @ 0.6	2.9 – 3.2	2.9	7.5 @ 1	2	18	0.07	-1.6
[14] MWCL'14	180nm	dc – 1.4	1.4	16.4 @ 0.1	3 – 4.7	3	-11 @ 0.9	1.8	12.8	0.04	-24
[3] JSSC'04	250nm	0.02 – 1.6	1.6	13.7 @ 0.01	1.9 – 2.2	1.9	0 @ 0.9	1.6	28.5	0.043	-6.1

* $FOM = 20log_{10}(\frac{IIP3[mW]\times Gain[lin]\times BW[GHz]}{P_{dc}[mW]\times(NF[lin]-1)})$ in [4].

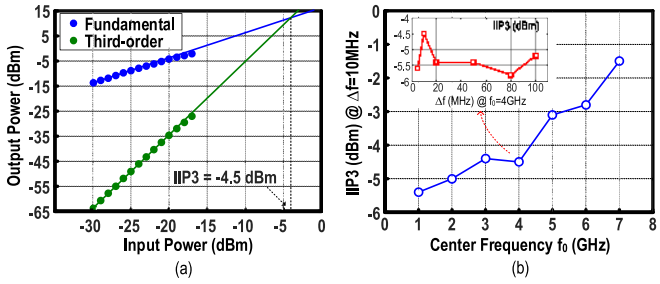

Fig. 10. (a) Measured IIP3 of the proposed LNA for two-tone inputs of 4 and 4.01 GHz and (b) Measured IIP3 versus center frequency (f_0) and two-tone separation (Δf) of the proposed LNA.

supply. Fig. 9 compares the calculated, simulated and measured results of S_{21}, NF and S_{11}. The peak S_{21} is 16.8 dB with a -3dB bandwidth (f_{-3dB}) of 7 GHz. S_{21} has a maximum in-band ripple of 0.32 dB. Measured NF_{min} and NF_{max} is 2.87 dB at 2 GHz, and 3.77 dB at 7 GHz. In-band variation of NF is only 0.84 dB from 0.5 to 7 GHz. The calculated results derived in Section II are consistent with the simulated and measured results. Fig. 10(a) shows that the measured IIP3 is -4.5 dBm, when two-tone signals at 4 and 4.01 GHz are applied. The frequency spacing Δf between the two-tone signals at 4 GHz is swept as shown in Fig. 10(b). The highest IIP3 is -4.5 dBm when the space is 10 MHz, and the lowest IIP3 is -5.8 dBm when the space is 80 MHz. IIIP3 is also measured across various center frequencies. IIP3 steadily increases with center frequency due to a lower gain at higher frequency. The highest IIP3 is -1.5 dBm at 7 GHz.

Table I benchmarks the performances with the prior art. This brief has low-and-flat NF, high gain and better overall FOM. Although inductors are applied, the area is still comparable to other works without passive inductors [4], [8], [14].

V. CONCLUSION

This Brief has described a wideband noise-cancelling LNA using resistor plus source-follower feedback to enhance the gain and NF. The design principles and parameter tradeoff have been analyzed in detail, and the analysis is consistent with both the simulation and measurement results. The LNA prototype fabricated in 65-nm CMOS shows a competitive performance with respect to the state-of-the-art.

REFERENCES

[1] S. Stroh, "Ultra-wideband: Multimedia unplugged," *IEEE Spectr.*, vol. 40, no. 9, pp. 23–27, Sep. 2003.

[2] C.-F. Liao and S.-I. Liu, "A broadband noise-canceling CMOS LNA for 3.1–10.6-GHz UWB receivers," *IEEE J. Solid-State Circuits*, vol. 42, no. 2, pp. 329–339, Feb. 2007.

[3] F. Bruccoleri, E. A. M. Klumperink, and B. Nauta, "Wide-band CMOS low-noise amplifier exploiting thermal noise canceling," *IEEE J. Solid-State Circuits*, vol. 39, no. 2, pp. 275–282, Feb. 2004.

[4] K.-H. Chen and S.-I. Liu, "Inductorless wideband CMOS low-noise amplifiers using noise-canceling technique," *IEEE Trans. Circuits Syst. I, Reg. Papers*, vol. 59, no. 2, pp. 305–314, Feb. 2012.

[5] H. Lee, T. Chung, H. Seo, I. Choi, and B. Kim, "A wideband differential low-noise-amplifier with IM3 harmonics and noise canceling," *IEEE Micow. Wireless Compon. Lett.*, vol. 25, no. 1, pp. 46–48, Jan. 2015.

[6] X. Wang, W. Aichholzer, and J. Sturm, "A resistive feedback LNA with feedforward noise and distortion cancellation," in *Proc. Eur. Solid-State Circuits Conf. (ESSCIRC)*, Sep. 2010, pp. 406–409.

[7] M. M. Reja, K. Moez, and I. Filanovsky, "An area-efficient multistage 3.0- to 8.5-GHz CMOS UWB LNA using tunable active inductors," *IEEE Trans. Circuits Syst. II, Exp. Briefs*, vol. 57, no. 8, pp. 587–591, Aug. 2010.

[8] Y.-H. Yu, Y.-S. Yang, and Y.-J. E. Chen, "A compact wideband CMOS low noise amplifier with gain flatness enhancement," *IEEE J. Solid-State Circuits*, vol. 45, no. 3, pp. 502–509, Mar. 2010.

[9] W.-H. Chen, G. Liu, B. Zdravko, and A. M. Niknejad, "A highly linear broadband CMOS LNA employing noise and distortion cancellation," *IEEE J. Solid-State Circuits*, vol. 43, no. 5, pp. 1164–1176, May 2008.

[10] B. Guo, J. Chen, L. Li, H. Jin, and G. Yang, "A wideband noise-canceling CMOS LNA with enhanced linearity by using complementary nMOS and pMOS configurations," *IEEE J. Solid-State Circuits*, vol. 52, no. 5, pp. 1331–1344, May 2017.

[11] M. Parvizi, K. Allidina, and M. N. El-Gamal, "An ultra-low-power wideband inductorless CMOS LNA with tunable active shunt-feedback," *IEEE Trans. Microw. Theory Techn.*, vol. 64, no. 6, pp. 1843–1853, Jun. 2016.

[12] J. Kim, S. Hoyos, and J. Silva-Martinez, "Wideband common-gate CMOS LNA employing dual negative feedback with simultaneous noise, gain, and bandwidth optimization," *IEEE Trans. Microw. Theory Techn.*, vol. 58, no. 9, pp. 2340–2351, Sep. 2010.

[13] D. Im, "A +9dbm output P_{1dB} active feedback CMOS wideband LNA for SAW-less receivers," *IEEE Trans. Circuits Syst. II, Exp. Briefs*, vol. 60, no. 7, pp. 377–381, Jul. 2013.

[14] J. Y.-C. Liu, J.-S. Chen, C. Hisa, P.-Y. Yin, and C.-W. Lu, "A wideband inductorless single-to-differential LNA in 0.18 μm CMOS technology for digital TV receivers," *IEEE Microw. Wireless Compon. Lett.*, vol. 24, no. 7, pp. 472–474, Jul. 2014.

[15] B. Razavi, *RF Microelectronics*, 2nd ed. New York, NY, USA: Prentice-Hall, 2012, pp. 269–271.